How do Armed Conflict Transfer? Physical Modeling of Spatial Diffusion and Relocation in Prediction

Hao Sha[1*], Jingtian Hu[2*], Pengfei Tian[3*], Yue He[4],
Chong Chen[1], Fan Yang[5], Andre Python[6], Peng Cui[4†],

[1]Xingjian College, Tsinghua University
[2]Department of International Relations, Tsinghua University
[3]Qiuzhen College, Tsinghua University
[4]Department of Computer Science and Technology, Tsinghua University
[5]Yau Mathematical Science Center, Tsinghua University
[6]Center for Data Science, Zhejiang University

[*]These authors contributed equally to this research.
[†]To whom correspondence should be addressed; E-mail: cuip@tsinghua.edu.cn.

Despite a global decline in battle-related fatalities, the escalating frequency and intensity of civil conflicts underline the pressing need for high-accuracy and high-resolution forecasting to enhance local security measures. Traditional data-driven models often neglect the theoretical underpinnings of conflict dynamics and simplify crucial variables like spatiotemporal dependencies in a static, isolated manner. This study introduces *ConflictNet*, a new predictive model that gives a physical modeling of the spatiotemporal dynamics of political violence in a rigorous mathematical form. Using a dataset from the Middle East and Africa, our model outperforms the existing benchmark by 56% in accuracy.

In the 21st century, more than 40 major armed conflicts have scarred the global landscape, affecting the lives of over two billion people across different continents. These conflicts are not isolated events but systemic crises that result in widespread loss of life and extensive social and economic disruption. They undermine infrastructures, displace populations, and erode the foundations of human security (*1*). This complex web of consequences highlights the urgent need for innovative and effective conflict management strategies that can anticipate and mitigate these disturbances. Advanced surveillance systems, capable of gathering comprehensive, real-time data on economic fluctuations, political unrest, and social tensions, promise to revolutionize our approach to conflict prediction and intervention, potentially transforming the reactive nature of current conflict resolution strategies into proactive and preventive action (*2, 3*).

Conflict forecasting has traditionally held a central position in security studies. It has evolved from early reliance on game theory (*4, 5*) to incorporating sophisticated machine learning algorithms, a shift marked by seminal contributions by Ward et al (*1*). Particularly noteworthy is the advancement made by the Violence Early Warning System (ViEWS) project (*6–8*), which has utilized machine learning techniques in conjunction with social science theoretical variables to enhance the accuracy of political violence forecasts at the country-month level. With the advancement in spatial data and methodological quality, the feasibility of forecasting at a finer spatial and temporal resolution, particularly at the PRIO-GRID ($0.5^\circ * 0.5^\circ$) month level, is gradually being realized (*9, 10*). Python et al. (*11*) present a new framework that leverages Extreme Gradient Boosting (XGB), and Random Forest (RF) algorithm to predict terrorism ranking among the top performers in the traditional machine learning track.

Despite these technological and methodological advances, a significant gap persists in our predictive capabilities and understanding, especially regarding the complex interplay between natural and social factors at the local level. The simplifications inherent in current methodologies and the challenges of bottom-up data analysis and modeling are the main causes (*12, 13*).

Traditional models often rely on simplistic proxies, such as the dummy variable for neighborly relations or the relevant spatial lag features derived from the Correlates of War database, to infer interaction probabilities (*14*). These approaches inadequately capture the complex dynamics at play, leaving substantial room for improvement in both the spatial and temporal accuracy of predictions (*15, 16*).

To address existing gaps in conflict prediction, recent studies have increasingly leveraged deep learning techniques, which are particularly adept at capturing the complex spatiotemporal dependencies that are characteristic of conflict data. The incorporation of sophisticated models such as recurrent neural networks (RNNs) (*17*), long-short term memory networks (LSTMs) (*18*), graph convolutional networks (GCNs) (*19*), and spatiotemporal graph neural networks (STGNNs) (*20*) has significantly enhanced our understanding of conflict dynamics. These models are adept at processing massive datasets to discern subtle patterns and interactions, thus offering a more dynamic and detailed view of conflict scenarios (*21–23*). The integration of these cutting-edge computational tools allows researchers to explore the nuanced implications of various predictors and their interrelationships across time and space, providing a robust framework for more accurate conflict predictions (*24–28*).

Despite these advancements, the inherent 'black box' nature of deep learning models poses significant challenges to interpretation and explanation, which are crucial for their application in real-world scenarios (*29*). To overcome these limitations, there has been a push towards integrating physical principles into the design and training of these models. This approach involves using physical or knowledge-assisted models to initialize and structure the neural networks, thus enhancing their transparency and interpretability (*30–32*). For instance, incorporating models of chaotic physical dynamics has shown promise in improving predictions in areas such as extreme weather events (*33*), thereby mirroring potential applications in conflict prediction (*34*).

ConflictNet

Accurate real-time conflict prediction requires deep understanding and rigorous modeling of conflict displacement and proliferation. ConflictNet provides such a rigorous modeling using partial differential equations (PDEs) and embedded in a neural network for solution. Previous literature suggests that a diffuse phenomenon (*35–37*) exists in conflict elements $u \in \mathbb{R}^n$ such as personnel, weaponry, and supplies. We validate this phenomenon in historical African conflict data (*6–8*), as shown in Figure 1a. Thus, after giving simple particle and mechanistic assumptions on the conflict elements, we can derive the following PDE describing their diffusion:

$$\frac{\partial u_i}{\partial t} = \sum_{j=1}^{n} \xi_{ji} \nabla \cdot (D_i \nabla u_i - u_j \mu_j \nabla \phi). \tag{1}$$

In the derivation, we naturally obtain a set of variables, D_i, μ_j, and ϕ, that describe the intrinsic properties of the region. In previous studies, this lack of invariance resulted in models that lacked time consistency and stability. ConflictNet addresses this problem by constraining the consistency of these variables over short time spans, while explaining regional characteristics and providing new perspectives on the conflict intervention. Given the current $u(t)$, diffusion modules estimate intrinsic variables D_i, μ_j, ϕ and compute the predicted value $u(t + \delta t)$ based on Equation 6.

Diffusion is not the only property of conflict elements transfer. Studies in recent years have shown that the overall coupling of conflict elements transfer is greater than the diffusivity of the particles modeled above. We model this tendency as rigid-body motion and use Newtonian mechanics to calculate the distance X over which u_i moves under the potential field ϕ as $X = \int v_{i,0} dt + \frac{\mu_i \nabla \phi}{2u_i}(dt)^2$. It is worth noting that rigit modules only estimate initial velocity $v_{i,0}$ and share intrinsic variables D_i, μ_j, and ϕ with diffusion modules to maintain spatial consistency.

Ultimately, ConflictNet estimates the mixing ratio p to fuse particle diffusion u_i^{df} and rigid motion u_i^{rm}, while considering the residual term q_i to characterize the self-generation and ex-

tinction of the conflict elements as $\frac{\partial u_i}{\partial t} = p_i \frac{\partial u_i^{df}}{\partial t} + (1 - p_i) \frac{\partial u_i^{rm}}{\partial t} + q_i$. Multimodal explicit modeling of conflict transfer allows for theoretical assurance of ConflictNet's predictions of spatio-temporal interactions of conflict, and the naturally derived intrinsic variables in the modeling describe the regional invariance of conflict factors thus providing new perspectives on the conflict intervention.

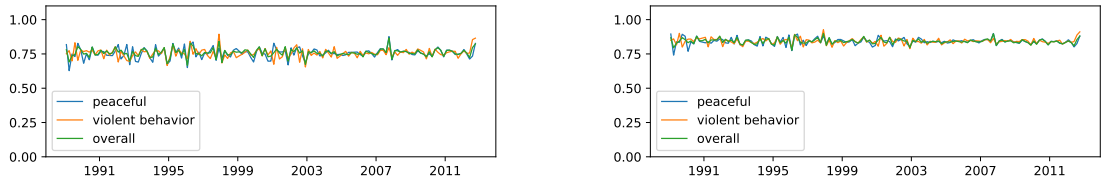

(a) The region ratio that the feature value regress to local mean

(b) The region ratio that the feature value pule potential field regress to local mean

Figure 1: We compute the ratio of whether the next time region value is between the current region value and current local region value mean in two months (based on local radius choice, and we draw three versions: peaceful protests, protests with violent behavior, and overall protests.

Model Evaluation

Baselines and metrics. To establish benchmarks, we implemented a broad spectrum of forecasting models, including classic machine learning models (*7, 8, 11*), temporal deep learning models (*17, 18, 21*), graph-based models (*19, 22*), and spatiotemporal deep learning models (*20, 23*).

For cross-validation, we chose 2013, 2016, and 2019 as checkpoint years. Each checkpoint utilized a 24-month evaluation period, with forecast horizons (h) set at 1, 3, 6, and 9 months, ensuring a thorough assessment across varying temporal scales. The model performance is summarized in Table 1, showing metrics such as Area Under Precision-Recall Curve (PR-AUC), Area Under Receiver Operating Characteristic Curve (ROC-AUC), and F_1 Score.

Our model significantly outperforms the baselines across all metrics. It effectively models

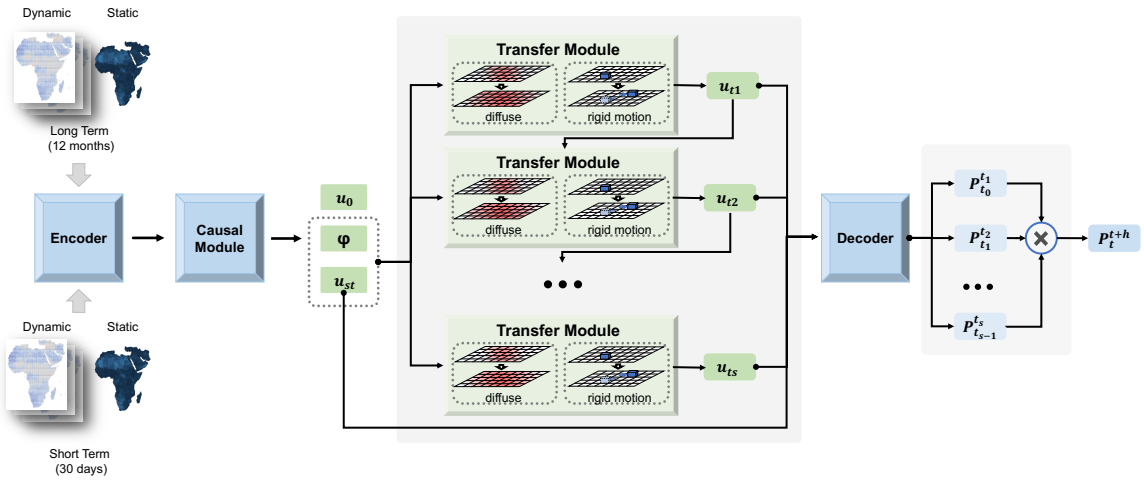

Figure 2: Framework of ConflictNet. The encoder integrates dynamic and static features, extracting long-term trends and immediate patterns; the transfer module and decoder solve the PDEs for the transfer of conflict factors and output the resultant probability of conflict.

conflict diffusion mechanisms within latent spaces, achieving superior ROC-AUC scores, and capturing more positive examples, as reflected in PR-AUC and F_1 scores, compared to models relying solely on direct spatiotemporal coupling. Temporal deep learning models did not show significant improvement over classic machine learning approaches, likely due to overfitting and the challenges of optimizing complex models with limited data. Graph-based models showed modest success, underscoring the importance of spatial relationships in conflict dynamics. The use of average pooling to incorporate temporal information, though minimal, highlighted the relevance of time in conflict prediction. Spatiotemporal deep learning models performed better than other baselines by integrating both spatial and temporal data, yet they fell short of our approach. Their complex black-box nature makes optimization challenging, underscoring the benefits of our explicit modeling of spatiotemporal relationships.

Robustness checks. The results of our ablation studies, detailed in Table 3, underscore the critical contributions of individual model components. Removing the causal module led to a noticeable decrease in all performance metrics, underscoring its pivotal role in refining causal

Table 1: Performance of different methods with $h = 1, 3, 6, 9$ months. We selected three historical periods for cross-validation: 2013, 2016, and 2019, taking 24 months at a time, and the table shows the average values. Bold face indicates the best result of each column and underlined is the second-best.

	PR-AUC %(↑)				ROC-AUC %(↑)				F_1 %(↑)			
	1	3	6	9	1	3	6	9	1	3	6	9
ViEWS	36.4	32.8	31.0	29.9	94.8	92.2	90.4	88.6	34.7	31.4	29.6	28.8
XGBoost	37.4	33.1	30.8	30.1	93.9	93.1	92.4	91.6	35.4	31.4	28.7	27.3
RNN	33.4	29.7	29.1	28.6	92.1	91.6	91.4	91.3	35.7	33.6	32.4	31.9
GRU	35.8	31.5	30.2	29.9	92.2	91.3	91.0	90.8	39.5	36.4	35.8	35.4
LSTM	36.2	32.1	30.1	29.4	92.3	92.0	91.5	91.2	39.4	36.6	35.5	34.8
GCN	35.6	31.2	29.7	28.7	91.8	91.1	90.8	90.5	39.8	36.4	35.5	35.0
GAT	38.9	34.4	32.7	31.5	94.3	94.0	93.5	93.2	40.6	36.1	36.4	35.8
STSGCN	42.6	38.5	35.4	32.7	95.1	94.8	94.6	94.4	42.4	37.2	35.2	36.1
STGNN	43.3	39.2	35.4	31.9	95.2	95.0	94.6	93.9	42.5	38.3	36.1	35.9
ConflictNet	**56.7**	**51.2**	**48.8**	**47.6**	**97.0**	**96.6**	**96.3**	**96.2**	**53.7**	**50.0**	**48.2**	**47.5**

relationships and mitigating the confounding effects of historical and geographical factors on feature representation. Similarly, the exclusion of the transfer module resulted in a significant performance drop to baseline levels, affirming the efficacy of our physical modeling approach in elucidating conflict transfer dynamics and simplifying model optimization.

Detailed in Table 2, designing with a gaseous diffusion model alone would not be compatible with some of the characteristics of the armed conflict we are modeling, such as the fact that the gradient is not only determined by the concentration of the conflict factor (weaponry or armed personnel) but also by the strategic value of a given area or the ability of the governmental forces to repress it on the ground. This cannot be bridged with our reality, and we have also done this type of simplification prior to modeling to find that there is absolutely no way to capture the features and complete the task.

Factor Transfer Building upon the discussions in the last section, this study delves deeper into the spatial and temporal dynamics of conflicts, leveraging the capabilities of our Conflict-

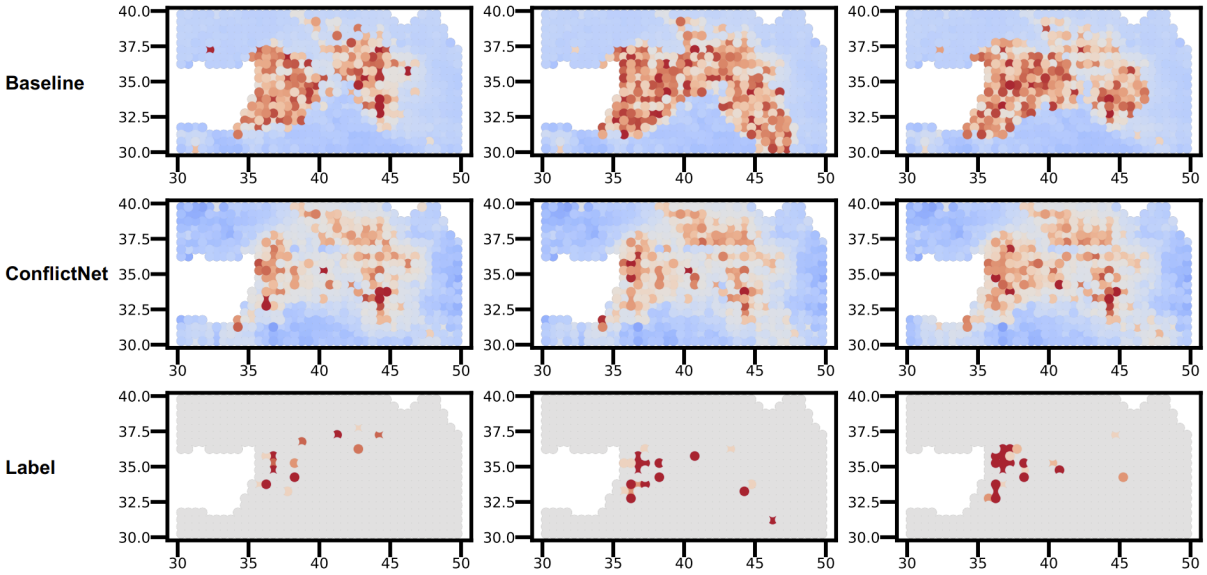

Figure 3: Thermodynamic diagrams depicting the baseline method or ConflictNet conflict factors, along with corresponding labels, in Damascus, Syria, every three months from June 2012 to June 2013. This figure displays the progression of conflict representation diffusion over time, segmented into three-month intervals starting from June 2012. The top row visualizes the diffusion patterns predicted by the baseline model, offering insight into its approach to modeling spatial transfer. The middle row illustrates the diffusion outcomes using our proposed ConflictNet model, highlighting its predictive performance in mapping conflict dynamics. The bottom row provides the actual conflict labels for the corresponding months, serving as a reference point for evaluating the accuracy of both models.

Net model. Figure 3 presents a focused analysis of a randomly selected localized area within Damascus, Syria, chosen from the broader map to scrutinize the spatio-temporal dynamics of conflict with greater detail. This selection allows for an in-depth comparison between the model predictions and actual conflict occurrences. The baseline model's estimations suggest a tendency towards an undifferentiated risk spreading, indiscriminately labeling adjacent grids to a conflict site as high-risk areas. This approach contrasts sharply with the observed patterns of conflict distribution. In comparison, ConflictNet's predictions demonstrate a higher congruence with the actual conflict labels, pinpointing high-risk areas with greater specificity. This nuanced identification of risk points reflects ConflictNet's advanced capability to discern the complex

Table 2: Data Temporally and Spatially Splitting. Temporally, we segmented the dataset at a critical point: October 2008. It was chosen based on a significant historical event, the Financial Crisis, which may shift in conflict dynamics because of the strategic contraction of the United States. Spatially, we divided the dataset using a latitude cut-off at 12°N.

Training	**Testing**	**Time**	**PR-AUC %**	**ROC-AUC%**	**F1%**
Spatial Splitting					
South	North	1	51.6	96.3	49.2
		9	39.2	95.5	43.9
Temporal Splitting					
Before 2008	After 2008	1	55.5	96.8	51.4
		9	44.8	96.0	46.1

Table 3: Ablation study. We forecast the 1st month ahead and perform 3-fold cross-validation. w/o causal is ConflictNet without Causal Module. w/o transfer is ConflictNet without Transfer Module.

	PR-AUC %(↑)	ROC-AUC %(↑)	F_1 %(↑)
ConflictNet	56.7	97.0	53.7
w/o causal	53.4	96.7	50.6
w/o transfer	40.3	94.9	39.1

dynamics of political violence. Moreover, ConflictNet estimates a sparser distribution of conflict grids compared to the baseline model, adhering more closely to the empirical understanding that instances of political violence are relatively rare events. This sparsity in predicted conflict zones underscores ConflictNet's refined approach to modeling the density and distribution of conflict occurrences.

Feature Importance Political scientists and policy-makers have long argued that state weakness leads to civil conflict while enhancing state power helps prevent violence. Why, then, has increased state capacity worldwide recently coincided with more civil conflicts? our model proves that enhanced state presence at the sub-national level—a symptom of growing state

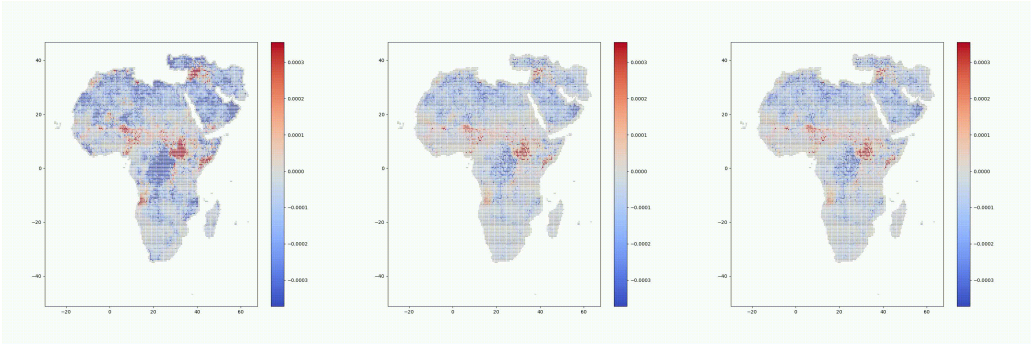

Figure 4: Spatial Heterogeneity in the Impact of State Capacity on Armed Conflict. At the red grids, a state extends its presence when its capacity grows. Within each state, such an increase of control in peripheral regions often encounters resistance from established local non-state powers, leading to civil conflict.

capacity—may induce violent resistance from the established nonstate powers such as local leaders and communities in the short term. Figure 4 and Figure 5 demonstrate that increased state presence triggers civil conflict, particularly in the first five years of such increasing state presence, and this effect is stronger in remote and ethnically heterogeneous regions. Evidence also suggests that ethnic groups settled in peripheral regions are prominent resisters to state penetration.

These results expand prior understanding of the impact of spreading state authority on political violence. Although scholars generally hold a positive view about expanding state governance, I show that states may break peace while pursuing prosperity. The reason—often ignored by existing literature—is that a relatively large increase of state power could transform local non-state actors into more violent ones. The Indians in Peru's Amazon forest became aggressive to the outsiders only after the oil industry barged into their region, bringing diseases and massive deaths in their community. Noticeably, this is not the case for all regions and is only applicable to those with pre-existing non-state powers. Furthermore, evidence only supports the provocation effect in the short term but not for a longer period. I emphasize these conditions here and suggest more attention to the heterogeneity at the sub-national level and

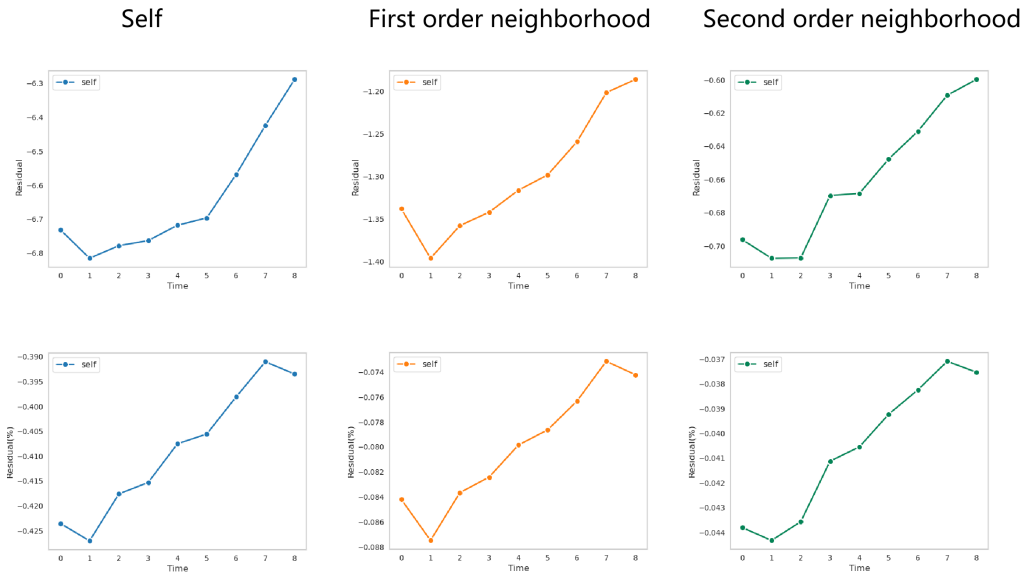

Figure 5: The Influence of State Capacity Decays Over Time. For the central government, the purpose of consolidating its peripheral territory is mainly resource and security, while conflict incidents are unintended consequences that would only occur when local non-state powers resist. This implies that the preexistence of non-state actors in local contexts and their ability to initiate conflict is vital to the provocation effect of increased state presence.

across time in conflict studies.

Conclusion

Predicting conflicts is a crucial endeavor with far-reaching implications for both human lives and financial resources. In our research, we focus on modeling the intricate spatiotemporal dependencies inherent in conflict prediction to elucidate its dynamic nature. By integrating these dynamic processes with Partial Differential Equation (PDE) models, we adopt a physical modeling approach that enhances our ability to capture the nuanced spatiotemporal characteristics effectively. Beyond its immediate application in conflict prediction, our methodology holds promise for addressing analogous challenges in social contexts or other dynamic predictive scenarios. Moreover, it contributes to a deeper comprehension of the underlying mechanisms driving conflicts. It provides valuable insights for conflict forecasting and paves the way for

utilizing physical models in future political science research to comprehend spatial dynamics of social phenomena.

Methods

Formulation and Data

Problem Formulation Our study represents the spatiotemporal domain using PRIO-GRID's regular grid cells, each measuring $0.5° * 0.5°$, allowing for the precise localization of political violence events (*38*), where political violence events can potentially occur and be reported with high spatial accuracy. The grid cells are replicated for each month from 1990 to 2020 across Africa, and each grid has features C_t at each time t. We classify grid features into dynamic categories, such as the number of protests, and static categories, like the percentage of mountainous terrain per cell, reflecting changing and constant elements within the analysis period. Utilizing historical data spanning the previous p months $\{C_{t-p}, ..., C_t\}$ for each grid cell, our objective focuses on accurately predicting the likelihood of conflict occurrence within a specified future month P_{t+h}^{t+h+1}.

Dataset Introduction We utilize a probabilistic graphical model (PGM) to depict the spatiotemporal domain, leveraging PRIO-GRID's high-resolution cells, with our study encompassing an extensive dataset of 4,785,150 monthly cells (13,110 grid cells × 365 months) across Africa. Our conflict event data is derived from the UCDP-GED database (*39*), supplemented by various feature data sources including PRIO-GRID (*38*), World Development Indicators, and information on political exclusion (*40*), demographic factors, protests (*41*), and institutional characteristics (*42*).

Data Motivated Observation We summarize the data characteristic from our exploration based on the dataset ViEWS (*6–8*). First, our initial observation identifies a local regression towards the mean for certain features, akin to the dynamic behavior observed in physical objects on varied terrains. For instance, features resembling natural disasters tend to regress to regional averages, mimicking the behavior of balls on a plane, see Figure 6. Other features like the forced migrants or protest events (*43*) perform like balls on the rugged mountain, the value of features plus the potential field value will most regress to the region mean next time step with higher probability. As shown in Figure 7, over 76% regions on average in the left panel and over 84% regions on average in the right panel regress to the local mean.

Second, we note the transformative nature of certain features, like troop movements, which are inherently constrained by the physical space, necessitating their analysis as complete entities moving within that space. (*37*). Lastly, we delve into the concept of feature coupling, recognizing that conflict emergence is often the result of complex interplays among multiple factors. Our study particularly focuses on the intertwined roles of opportunity, greed, and grievance (*40, 44, 45*) in civil conflict onset, as evidenced by the correlation matrix showcasing feature interdependencies. However, the academic community still lacks a definitive answer about which is more likely to lead to violent conflicts, as these three factors are often closely intertwined. The correlation matrix, depicted in Figure 8, reveals intricate coupling relationships among the features, particularly between natural disasters and land types.

Physical Modeling

Traditional approaches in machine learning have primarily conceptualized the spatiotemporal dynamics of armed conflict through diffusion models focused on conflict intensity levels. These models examine how the likelihood of conflict emergence spreads across regions. Recent advancements in international relations theory, however, emphasize the spatial diffusion

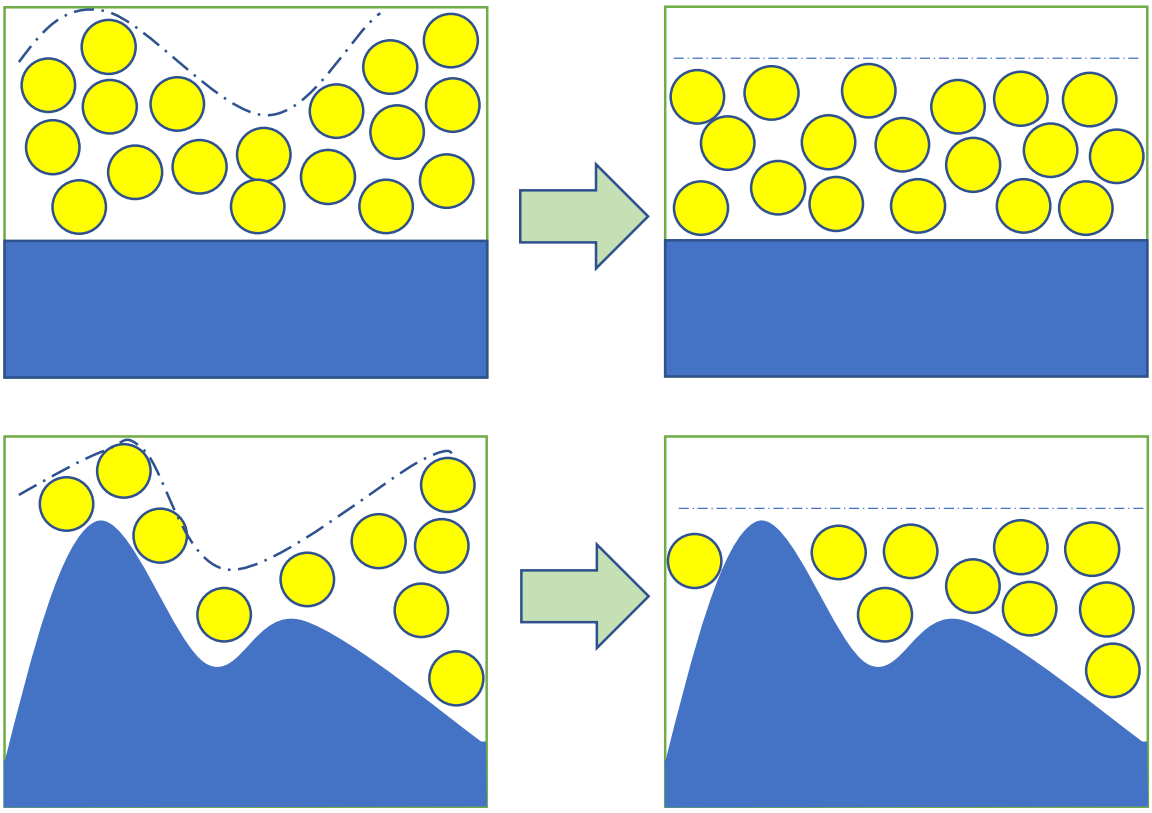

Figure 6: Balls on plains or mountains. The first row indicates that the conflict factor diffuses along its concentration gradient without considering the potential field; the second row indicates that under the influence of the potential field, the conflict factor diffuses to its concentration gradient force in equilibrium with the potential field force.

of conflict's underlying factors $u = (u_1, ..., u_n)$, such as movements of people, weapons, and information—arguing that these elements catalyze macro-level shifts in conflict dynamics (*36*).

In our analysis, we define "conflict factors" as the fundamental elements underlying potential conflict features, encompassing aspects like people, weaponry, and information dissemination. By drawing parallels to the physical diffusion processes observed in gases, we hypothesize that conflict factors similarly demonstrate spatial mobility and interact in a manner reminiscent of fluid viscosity. The movement of these conflict factors tends to reduce the concentration gradient within a given area. This tendency mirrors the principle of diffusion in physical systems.

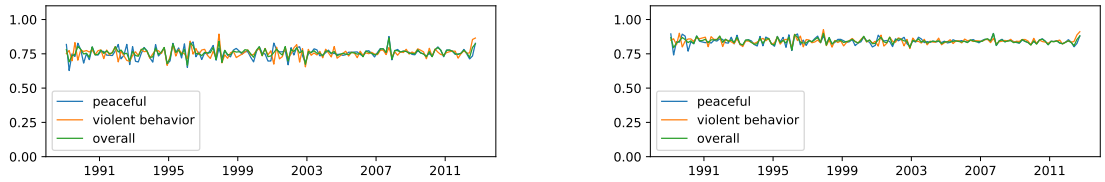

(a) The region ratio that the feature value regress to local mean

(b) The region ratio that the feature value pule potential field regress to local mean

Figure 7: We compute the ratio of whether the next time region value is between the current region value and current local region value mean in two months (based on local radius choice, and we draw three versions: peaceful protests, protests with violent behavior, and overall protests.

Therefore, we model the diffusion of feature $u_i(t, x, y)$ as follows:

$$\frac{\partial u_i}{\partial t} = \nabla \cdot (D_i \nabla u_i), \tag{2}$$

where $D_i(x, y)$ describes the difficulty of organizing conflict feature u_i. In the field of conflict studies, it is widely recognized that rebels often encounter a collective action problem. This consensus stems from the understanding that the public goods nature of insurgency creates varying levels of incentives for free-riding among potential participants. Additionally, the risks associated with individual engagement in collective insurgent action differ depending on the economic and social conditions prevalent in different regions. In other words, mobilizing potential armed troops and forces can pose varying levels of difficulty across different regions (*46, 47*).

Beyond individual feature diffusion, the transfer and spread of conflict features are profoundly influenced by the strategic significance of regional characteristics, i.e., conflict features will tend to transfer to regions with important strategic locations. To quantify the strategic importance of regions, we introduce a scalar potential field, $\phi(x, y)$, which serves as a metaphorical 'gravitational force' drawing conflict factors towards regions of high strategic value. Just as the ball slipped under gravity as demonstrated in Figure 6, the conflict factor will also move under the action of a potential force. In conflict contexts, the function $\phi(x, y)$ is used to represent a specific graphic character that describes the strategic significance and attractiveness of a partic-

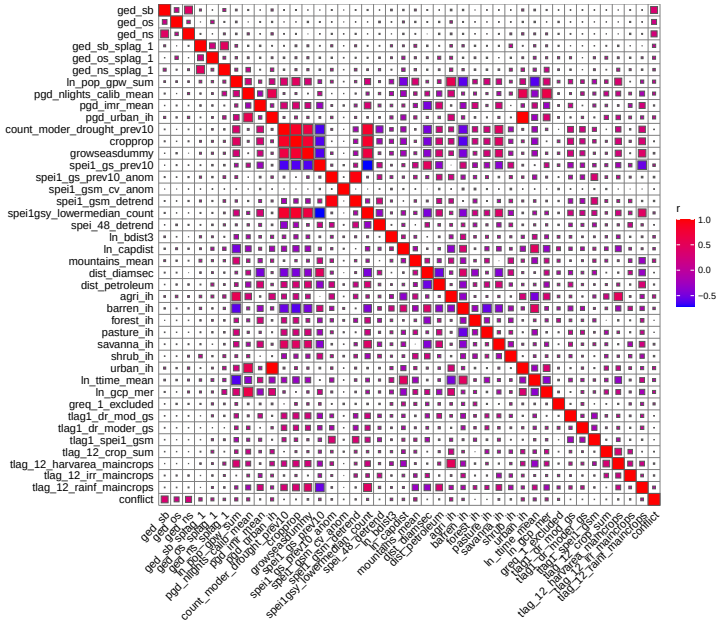

Figure 8: Correlation between each feature.

ular site. Through this function, we can identify certain regions that consistently serve as crucial battlegrounds. One such example is the Sahel region in East Africa, which has been recognized as a significant hotspot for conflicts (*48, 49*). The PDE is then modified as:

$$\frac{\partial u_i}{\partial t} = \nabla \cdot (D_i \nabla u_i - u_i \mu_i \nabla \phi), \tag{3}$$

In our model, $\mu_i(x, y)$ quantifies the influence of the potential field ϕ on the conflict feature u_i. This feature u_i represents the propensity for violence within a region, encapsulating the local population's inclination towards engaging in violent acts. (*50–52*).

Beyond the diffusion characteristics, over extended periods, the conflict factor demonstrates increased inseparability. For capturing the amalgamation of conflict factors over extended periods, we employ a spatial discretization strategy. This approach segments the spatial domain into a mesh grid, where each cell encapsulates conflict factors as discrete entities, enabling a more granular analysis of their dynamics. Consequently, the movement of these features is governed

by the rigid body motion equations:

$$\mu_i \nabla \phi = u_i a_i, \tag{4}$$

$$X = \int v_{i,0} dt + \frac{1}{2} a_i (dt)^2, \tag{5}$$

where $X = (x, y)$ is displacement of feature u_i, $v_{i,0} = (v_{i,0}^x, v_{i,0}^y)$ is initial velocity of feature u_i, $a_i = (a_i^x, a_i^y)$ is acceleration of feature u_i. In the actual solution, we discretize the integral equation (5).

Moreover, the coupling properties inherent among the conflict features necessitate consideration. The dynamics of both diffusion and rigid motion are fundamentally driven by responses to external forces, which, in the context of conflict dynamics, are typically represented by concentration gradients or potential fields. These gradients or fields act as proxies for the various pressures and incentives that influence the movement and interaction of conflict factors. The interaction among these factors, therefore, can be conceptualized as a superposition of forces acting upon them. Accordingly, this perspective necessitates a revision of the transfer equation previously introduced (3)(4):

$$\begin{aligned} \frac{\partial u_i}{\partial t} &= \sum_{j=1}^{n} \nabla \cdot (\xi_{ji} D_j \nabla u_j - u_j \xi_{ji} \mu_j \nabla \phi) \\ &= \sum_{j=1}^{n} \xi_{ji} \nabla \cdot (D_i \nabla u_i - u_j \mu_j \nabla \phi), \end{aligned} \tag{6}$$

$$\sum_{j=1}^{n} \xi_{ji} \mu_j \nabla \phi = u_i a_i, \tag{7}$$

where ξ_{ji} represents the effect of diffusion of u_j on u_i, $\xi_{ii} = 1$.

In addition to the diffusion of factors, they are self-generating and self-absorbing. Finally, considering both diffusion and rigid motion of features, the transfer equation is written as:

$$\frac{\partial u_i}{\partial t} = p_i \frac{\partial u_i^{df}}{\partial t} + (1 - p_i) \frac{\partial u_i^{rm}}{\partial t} + q_i, \tag{8}$$

where $\partial u_i^{df}/\partial t$ is the diffuse part of the feature given by equation (6), $\partial u_i^{rm}/\partial t$ is the rigid motion part of the feature given by equation (7) (5), p_i is mixing probability, q_i is self-generating (absorbing) of u_i.

Framework

Encoder As shown on the left side of Figure 2, we treat features in two categories according to their variability over time: features that do not change much over time are called static features and are encoded using GCN to capture spatial coupling; features that change a lot over time are called static features and are encoded using GCN and LSTM to capture spatiotemporal relationships. We coded both long and short-term information, extracting trends from coarse-grained long-time information at the month level and diffusion details from fine-grained short-time information at the day level.

Causal Module The causes of armed conflict are highly complex and are strongly influenced by historical periods and geographic characteristics, and the triggers of conflict vary from one historical period and geographical location to another. However, we expect to capture a universal law of transfer, an inherent pattern of conflict occurrence. Inspired by (*53*), we perform spatiotemporal debiasing of the features extracted by the encoder:

$$f_{db} \overset{Linear}{\approx} W_x f_b + W_s r_b \tag{9}$$

where f_b is biased feature, f_{ub} is debiased feature, W_x and W_s are learnable parameters. r_b is the debiasing factor and can be calculated using the following equation:

$$r_b = \sum_{i=1} \alpha_i s_i P(i) \tag{10}$$

where $s_i = {N_i}^{-1} \sum_{k=1}^{N_i} f_k^i$ is the average of features of all samples in category i, $P(i)$ is the proportion of category i in the total sample, α_i can be computed as follows:

$$\alpha_i = softmax(\frac{(W_q f_b)^T (W_k s_i)}{\sqrt{d_m}}) \tag{11}$$

where d_m is dimention of feature, W_q and W_k are learnable parameters. Thus, causal debiasing means categorizing the sample to reduce the differences in features due to differences in categories.

We de-bias time and space separately: Temporally, we divided into three historical periods with similar conflict triggers within each period (*7, 8*). Spatially, we divided the grid within a country into one category because of similar conflict triggers within the same country (*38*). In this way, we reduce the biased effect of the historical period and geographic location on feature extraction. After debiasing, we integrate and encode the above information through Multi-Layer Perception (MLP) to obtain the initial value of the dynamic factor u_0, the scalar potential field ϕ, and the static factor u_{st} without diffusion.

Transfer Module and Decoder As shown in Figure 2, the transfer module discretizes time and solves the PDE using an iterative approach to model the factor transfer process. We discretize the period between t and t+h into s time steps $\{t_1, ..., t_s\}$. For each time step t_k, since the conflict is caused by a combination of static and dynamic factors, we decode both using an MLP with shared weights to estimate the probability of a conflict occurring in that time interval, which in turn computes the total probability:

$$P_{t_{k-1}}^{t_k} = Sigmoid(MLP(u_{t_k}, u_{st})) \tag{12}$$

$$P_t^{t+h} = 1 - \prod_{k=1}^{s} (1 - P_{t_{k-1}}^{t_k}) \tag{13}$$

where $P_t^{t+h}(x, y)$ is the probability that a conflict will occur in the area at times t through $t + h$.The way we modeled all the variables in the PDE is shown in Table **??**. We optimize

$D_i(x, y)$ and $\mu_i(x, y)$ as model parameters because they are time-invariant and represent the geopathic properties of a region; whereas we decode $\phi(x, y)$ from the features and share it during the iteration process because we assume that the potential field is invariant in the short term.

Experiment Settings To construct the graph $\mathcal{G}(\mathcal{V}, \mathcal{E}, \mathcal{T})$, we treat each of the N grid cells as a node within $\mathcal{V}$. Nodes are interconnected based on geographic proximity, with each node linked to its nearest 24 neighbors, forming the edge set $\mathcal{E}$. This design captures the spatial interrelations essential for conflict prediction. The time dimension is represented by $\mathcal{T}$, encompassing T discrete time points across our study period.

We use data from the past $p = 12$ months $[t - 12, t]$ to predict the probability of conflict after h months, $h = 1, 3, 6, 9$. For the practical application of Partial Differential Equations (PDEs) in modeling conflict spread, we discretize temporal data by dividing each month into five equal segments. This approach enhances our model's temporal resolution, enabling a more detailed analysis of conflict dynamics over time. All the parameters are initialized with Glorot initialization, and we use Adam optimizer. We performed 3-fold cross-validation with the test set starting in Jan 2013, Jan 2016, and Jan 2019, and 24 months in length, the validation set is the 12 months before the test set starting point, and the rest as the training set. To rigorously evaluate our model's predictive performance, we employ ROC-AUC and PR-AUC metrics for assessing overall accuracy and sensitivity to positive cases, respectively. Additionally, the F_i-Score is utilized to balance precision and recall, providing a holistic view of model efficacy in predicting conflict occurrences. All programs are implemented using Python 3.8 and PyTorch 1.11.0 with CUDA 11.8 in the ubuntu20.04 system with RTX4090 NVIDIA GPU devices.

Optimization

Our task is to predict the probability of a conflict, a binary classification problem. Since conflicts are sparse and the vast majority of samples are negative, we use Focal Loss (*54*) for binary classification optimization problems with biased samples:

$$\begin{aligned}\mathcal{L}_{fl} = \sum_{j=1}^{N} &- \alpha y(1 - P_{t,j}^{t+h})^{\gamma} log(P_{t,j}^{t+h}) \\ &+ (1-\alpha)(1-y)(P_{t,j}^{t+h})^{\gamma} log(1 - P_{t,j}^{t+h})\end{aligned} \tag{14}$$

where $P_{t,j}^{t+h} = P_t^{t+h}(x_j, y_j)$, α and γ are hyperparameters.

In practical applications, we are more concerned about the ability of the mod to find out the positive samples. In order to enhance this capability and at the same time speed up training, we modified Smooth AP loss (*55*) using fast-soft-rank (*56*):

$$\mathcal{L}_{ap} = 1 - \frac{1}{\|S_P\|} \sum_{P_t^{t+h} \in S_P} \frac{\mathcal{R}(P_t^{t+h}, S_P)}{\mathcal{R}(P_t^{t+h}, S_\Omega)} \tag{15}$$

where $\mathcal{R}(P_t^{t+h}, S_P)$ is is the rank of P_t^{t+h} in the set S_P, $\mathcal{R}$is fast-soft-rank which makes the sorting operation differentiable, S_P is the set of positive sample, and S_Ω is full set.

To ensure the continuity and robustness of the model in time, we want the model to have the same diffusion results from different temporal starting points to the same temporal end point. Therefore, we use the following loss function:

$$\mathcal{L}_{cyc} = \sum_{i=1}^{n} \|u_i(u_i(t), t+h) - u_i(u_i(t-1), t+h)\|_2 \tag{16}$$

where $u_i(u_i(t), t+h)$ means the result of diffusion from $u_i(t)$ at time t as a starting point to time $t+h$.

In the short term, we assume that conflict transfers dominate and therefore include the following regularization term:

$$\mathcal{L}_{rg} = \sum_{i=1}^{n} \sum_{j=1}^{N} \sum_{k=1}^{s} |q_i(t_k, x_j, y_j)| \tag{17}$$

Finally, the loss function is:

$$\mathcal{L} = \beta_{fl}\mathcal{L}_{fl} + \beta_{ap}\mathcal{L}_{ap} + \beta_{cyc}\mathcal{L}_{cyc} + \beta_{rg}\mathcal{L}_{rg} \tag{18}$$

References and Notes

1. M. D. Ward, B. D. Greenhill, K. M. Bakke, *Journal of Peace Research* **47**, 363 (2010).

2. N. B. Weidmann, M. D. Ward, *Journal of Conflict Resolution* **54**, 883 (2010).

3. M. D. Ward, *et al.*, *International Studies Review* **15**, 473 (2013).

4. N. W. Metternich, C. Dorff, M. Gallop, S. Weschle, M. D. Ward, *American Journal of Political Science* pp. n/a–n/a (2013).

5. B. B. de Mesquita, J. D. Morrow, E. R. Zorick, *American Political Science Review* **91**, 15 (1997).

6. H. Hegre, N. W. Metternich, H. M. Nygård, J. Wucherpfennig, *Journal of Peace Research* **54**, 113 (2017).

7. H. Hegre, *et al.*, *Journal of Peace Research* **56**, 155 (2019).

8. H. Hegre, *et al.*, *Journal of Peace Research* **58**, 599 (2021).

9. S. Schutte, J. Vestby, J. Carling, H. Buhaug, *Nature Communications* **12**, 2067 (2021).

10. S. Michelini, B. Šedová, J. Schewe, K. Frieler, *Humanities and Social Sciences Communications* **10**, 522 (2023).

11. A. Python, *et al.*, *Science Advances* **7**, eabg4778 (2021).

12. L.-E. Cederman, N. B. Weidmann, *Science* **355**, 474 (2017).

13. S. J. Cranmer, B. A. Desmarais, *Political Analysis* **25**, 145 (2017).

14. H. Mueller, C. Rauh, *American Political Science Review* **112**, 358 (2018).

15. D. Muchlinski, D. Siroky, J. He, M. Kocher, *Political Analysis* **24**, 87 (2016).

16. Y. Wang, *Political Analysis* **27**, 107 (2019).

17. A. A. Ballakur, A. Arya, *2020 5th International Conference on Computing, Communication and Security (ICCCS)* (2020), pp. 1–7.

18. S. Hochreiter, J. Schmidhuber, *Neural Computation* **9**, 1735 (1997).

19. B. Jiang, Z. Zhang, D. Lin, J. Tang, B. Luo, *2019 IEEE/CVF Conference on Computer Vision and Pattern Recognition (CVPR)* (2019), pp. 11305–11312.

20. B. Su, W. Zheng, *2020 Eighth International Conference on Advanced Cloud and Big Data (CBD)* (2020), pp. 119–124.

21. L. R. Medsker, L. Jain, *Design and Applications* **5**, 2 (2001).

22. P. Veličković, *et al.*, Graph attention networks (2018).

23. C. Song, Y. Lin, S. Guo, H. Wan, *AAAI Conference on Artificial Intelligence* (2020).

24. H. Hegre, P. Vesco, M. Colaresi, *International Interactions* **48**, 521 (2022).

25. T. Chadefaux, *International Interactions* **48**, 633 (2022).

26. A. Lindholm, J. Hendriks, A. Wills, T. B. Schön, *International Interactions* **48**, 759 (2022).

27. B. J. Radford, *International Interactions* **48**, 739 (2022).

28. P. T. Brandt, *et al.*, *International Interactions* **48**, 800 (2022).

29. B. Kim, F. Doshi-Velez, *ICML Tutorial on interpretable machine learning* (2017).

30. P. Raccuglia, *et al.*, *Nature* **533**, 73 (2016).

31. J. Hermann, Z. Schätzle, F. Noé, *Nature Chemistry* **12**, 891 (2020).

32. D. Pfau, J. S. Spencer, A. G. D. G. Matthews, W. M. C. Foulkes, *Physical Review Research* **2**, 033429 (2020).

33. Y. Zhang, *et al.*, *Nature* **619**, 526 (2023).

34. A. Zammit-Mangion, M. Dewar, V. Kadirkamanathan, G. Sanguinetti, *Proceedings of the National Academy of Sciences* **109**, 12414 (2012).

35. S. Schutte, N. B. Weidmann, *Political Geography* **30**, 143 (2011).

36. C. Dorff, M. Gallop, S. Minhas, *International Studies Quarterly* **66**, sqab086 (2022).

37. B. A. Most, H. Starr, *American Political Science Review* **74**, 932 (1980).

38. A. F. Tollefsen, H. Strand, H. Buhaug, *Journal of Peace Research* **49**, 363 (2012).

39. R. Sundberg, E. Melander, *Journal of Peace Research* **50**, 523 (2013).

40. L.-E. Cederman, N. B. Weidmann, K. S. Gleditsch, *American Political Science Review* **105**, 478 (2011).

41. C. Raleigh, r. Linke, H. Hegre, J. Karlsen, *Journal of Peace Research* **47**, 651 (2010).

42. S. I. Lindberg, M. Coppedge, J. Gerring, J. Teorell, *Journal of Democracy* **25**, 159 (2014). Publisher: Johns Hopkins University Press.

43. E. G. Rød, H. Hegre, M. Leis, *Journal of Peace Research* p. 00223433231186452 (2023).

44. P. Collier, A. Hoeffler, *Oxford Economic Papers* **50**, 563 (1998). _eprint: https://academic.oup.com/oep/article-pdf/50/4/563/6968570/50-4-563.pdf.

45. J. D. Fearon, D. D. Laitin, *American Political Science Review* **97**, 75 (2003).

46. C. Linebarger, *International Interactions* **41**, 583 (2015).

47. P. Vesco, *et al.*, *International Interactions* **48**, 860 (2022).

48. A. Braithwaite, *Conflict Hot Spots: Emergence, Causes and Consequences* (Routledge, London, 2016).

49. V. Sticher, J. D. Wegner, B. Pfeifle, *PNAS Nexus* **2**, pgad181 (2023).

50. T. R. Gurr, W. H. Moore, *American Journal of Political Science* **41**, 1079 (1997). Publisher: [Midwest Political Science Association, Wiley].

51. A. M. Matanock, *International Security* **41**, 93 (2017).

52. K. Sawyer, T. M. Andrews, *International Interactions* **46**, 872 (2020).

53. Y. Chen, D. Chen, T. Wang, Y. Wang, Y. Liang, *ArXiv* **abs/2204.07935** (2022).

54. T.-Y. Lin, P. Goyal, R. Girshick, K. He, P. Dollár, *2017 IEEE International Conference on Computer Vision (ICCV)* (2017), pp. 2999–3007.

55. A. Brown, W. Xie, V. Kalogeiton, A. Zisserman, *Computer Vision – ECCV 2020*, A. Vedaldi, H. Bischof, T. Brox, J.-M. Frahm, eds. (Springer International Publishing, Cham, 2020), pp. 677–694.

56. M. Blondel, O. Teboul, Q. Berthet, J. Djolonga (2020).

References and Notes

1. M. D. Ward, B. D. Greenhill, K. M. Bakke, *Journal of Peace Research* **47**, 363 (2010).
2. N. B. Weidmann, M. D. Ward, *Journal of Conflict Resolution* **54**, 883 (2010).
3. M. D. Ward, *et al.*, *International Studies Review* **15**, 473 (2013).
4. N. W. Metternich, C. Dorff, M. Gallop, S. Weschle, M. D. Ward, *American Journal of Political Science* pp. n/a–n/a (2013).
5. B. B. de Mesquita, J. D. Morrow, E. R. Zorick, *American Political Science Review* **91**, 15 (1997).
6. H. Hegre, N. W. Metternich, H. M. Nygård, J. Wucherpfennig, *Journal of Peace Research* **54**, 113 (2017).
7. H. Hegre, *et al.*, *Journal of Peace Research* **56**, 155 (2019).
8. H. Hegre, *et al.*, *Journal of Peace Research* **58**, 599 (2021).
9. S. Schutte, J. Vestby, J. Carling, H. Buhaug, *Nature Communications* **12**, 2067 (2021).
10. S. Michelini, B. Šedová, J. Schewe, K. Frieler, *Humanities and Social Sciences Communications* **10**, 522 (2023).
11. A. Python, *et al.*, *Science Advances* **7**, eabg4778 (2021).
12. L.-E. Cederman, N. B. Weidmann, *Science* **355**, 474 (2017).
13. S. J. Cranmer, B. A. Desmarais, *Political Analysis* **25**, 145 (2017).
14. H. Mueller, C. Rauh, *American Political Science Review* **112**, 358 (2018).
15. D. Muchlinski, D. Siroky, J. He, M. Kocher, *Political Analysis* **24**, 87 (2016).
16. Y. Wang, *Political Analysis* **27**, 107 (2019).
17. A. A. Ballakur, A. Arya, *2020 5th International Conference on Computing, Communication and Security (ICCCS)* (2020), pp. 1–7.
18. S. Hochreiter, J. Schmidhuber, *Neural Computation* **9**, 1735 (1997).
19. B. Jiang, Z. Zhang, D. Lin, J. Tang, B. Luo, *2019 IEEE/CVF Conference on Computer Vision and Pattern Recognition (CVPR)* (2019), pp. 11305–11312.
20. B. Su, W. Zheng, *2020 Eighth International Conference on Advanced Cloud and Big Data (CBD)* (2020), pp. 119–124.

21. L. R. Medsker, L. Jain, *Design and Applications* **5**, 2 (2001).

22. P. Veličković, *et al.*, Graph attention networks (2018).

23. C. Song, Y. Lin, S. Guo, H. Wan, *AAAI Conference on Artificial Intelligence* (2020).

24. H. Hegre, P. Vesco, M. Colaresi, *International Interactions* **48**, 521 (2022).

25. T. Chadefaux, *International Interactions* **48**, 633 (2022).

26. A. Lindholm, J. Hendriks, A. Wills, T. B. Schön, *International Interactions* **48**, 759 (2022).

27. B. J. Radford, *International Interactions* **48**, 739 (2022).

28. P. T. Brandt, *et al.*, *International Interactions* **48**, 800 (2022).

29. B. Kim, F. Doshi-Velez, *ICML Tutorial on interpretable machine learning* (2017).

30. P. Raccuglia, *et al.*, *Nature* **533**, 73 (2016).

31. J. Hermann, Z. Schätzle, F. Noé, *Nature Chemistry* **12**, 891 (2020).

32. D. Pfau, J. S. Spencer, A. G. D. G. Matthews, W. M. C. Foulkes, *Physical Review Research* **2**, 033429 (2020).

33. Y. Zhang, *et al.*, *Nature* **619**, 526 (2023).

34. A. Zammit-Mangion, M. Dewar, V. Kadirkamanathan, G. Sanguinetti, *Proceedings of the National Academy of Sciences* **109**, 12414 (2012).

35. S. Schutte, N. B. Weidmann, *Political Geography* **30**, 143 (2011).

36. C. Dorff, M. Gallop, S. Minhas, *International Studies Quarterly* **66**, sqab086 (2022).

37. B. A. Most, H. Starr, *American Political Science Review* **74**, 932 (1980).

38. A. F. Tollefsen, H. Strand, H. Buhaug, *Journal of Peace Research* **49**, 363 (2012).

39. R. Sundberg, E. Melander, *Journal of Peace Research* **50**, 523 (2013).

40. L.-E. Cederman, N. B. Weidmann, K. S. Gleditsch, *American Political Science Review* **105**, 478 (2011).

41. C. Raleigh, r. Linke, H. Hegre, J. Karlsen, *Journal of Peace Research* **47**, 651 (2010).

42. S. I. Lindberg, M. Coppedge, J. Gerring, J. Teorell, *Journal of Democracy* **25**, 159 (2014). Publisher: Johns Hopkins University Press.

43. E. G. Rød, H. Hegre, M. Leis, *Journal of Peace Research* p. 00223433231186452 (2023).

44. P. Collier, A. Hoeffler, *Oxford Economic Papers* **50**, 563 (1998). _eprint: https://academic.oup.com/oep/article-pdf/50/4/563/6968570/50-4-563.pdf.

45. J. D. Fearon, D. D. Laitin, *American Political Science Review* **97**, 75 (2003).

46. C. Linebarger, *International Interactions* **41**, 583 (2015).

47. P. Vesco, *et al.*, *International Interactions* **48**, 860 (2022).

48. A. Braithwaite, *Conflict Hot Spots: Emergence, Causes and Consequences* (Routledge, London, 2016).

49. V. Sticher, J. D. Wegner, B. Pfeifle, *PNAS Nexus* **2**, pgad181 (2023).

50. T. R. Gurr, W. H. Moore, *American Journal of Political Science* **41**, 1079 (1997). Publisher: [Midwest Political Science Association, Wiley].

51. A. M. Matanock, *International Security* **41**, 93 (2017).

52. K. Sawyer, T. M. Andrews, *International Interactions* **46**, 872 (2020).

53. Y. Chen, D. Chen, T. Wang, Y. Wang, Y. Liang, *ArXiv* **abs/2204.07935** (2022).

54. T.-Y. Lin, P. Goyal, R. Girshick, K. He, P. Dollár, *2017 IEEE International Conference on Computer Vision (ICCV)* (2017), pp. 2999–3007.

55. A. Brown, W. Xie, V. Kalogeiton, A. Zisserman, *Computer Vision – ECCV 2020*, A. Vedaldi, H. Bischof, T. Brox, J.-M. Frahm, eds. (Springer International Publishing, Cham, 2020), pp. 677–694.

56. M. Blondel, O. Teboul, Q. Berthet, J. Djolonga (2020).